NANO LETTERS

pubs.acs.org/NanoLett

Optical and Excitonic Properties of Crystalline ZnS Nanowires: Toward Efficient Ultraviolet Emission at Room Temperature

Rui Chen,[†] Dehui Li,[†] Bo Liu,[†] Zeping Peng,[†] Gagik G. Gurzadyan,[†] Qihua Xiong,*[,†,‡] and Handong Sun*[,†]

[†]Division of Physics and Applied Physics, School of Physical and Mathematical Sciences, Nanyang Technological University, Singapore 637371, Singapore, and [‡]Division of Microelectronics, School of Electrical and Electronics Engineering, Nanyang Technological University, Singapore 639798, Singapore

ABSTRACT A systematic investigation into the excitonic properties of wurtzite ZnS nanowires (NWs) is presented. Under optical excitation, the ZnS NWs exhibit strong ultraviolet (UV) emission. Optical transition from free exciton A, free exciton B, and shallow level emission are observed and analyzed through power-dependent and temperature-dependent photoluminescence spectroscopy measurements performed from 10 to 300 K. The excitonic transition and coupling strength of exciton-longitudinal optical phonon were directly determined from the evolution of exciton peak energy and peak width broadening. Our studies indicate that free excitons in ZnS nanowires are very stable, suggesting a great promise for high-efficiency light-emitting devices and lasers in the UV region. Finally, the carrier dynamics of the ZnS NWs were measured and analyzed for the first time by ultrafast spectroscopy.

KEYWORDS Nanowire, ZnS, photoluminescence, exciton

Recently, wide band gap semiconductor nanowires (NWs), e.g., ZnO, have received considerable attention due to their promising applications in highly efficient ultraviolet (UV) light sources (nanolasers),[1] waveguides, and photodetectors.[2−4] ZnS, another important II−VI group wide band gap polar semiconductor, has been most widely used for phosphor host,[5] optical coating, and solar cells.[6] Due to the wide band gap (3.68 eV for cubic phase and 3.70 eV for hexagonal-wurtzite phase at room temperature)[7] and relatively large exciton binding energy (40 meV),[8] ZnS is recognized as one of the most promising materials for a number of optoelectronic applications.[9] Especially, the emission wavelength of ZnS falls in the UV absorption band of most organics and biomolecules,[10,11] thus it is envisaged that ZnS NWs based devices may find applications in increasingly important fluorescence sensing of these species.

In order to achieve high efficiency room temperature photonic devices, it is important to have excitons existing up to room temperature. Moreover, superior crystalline quality is imperative to obtain efficient UV luminescence. Despite their advantageous band gap, bulk or thin film ZnS materials have not been able to be used for light-emitting devices due to a tendency of defect formation. ZnS in NWs form, on the other hand, may circumvent this difficulty, because very high crystalline quality can be readily achieved in one-dimensional vapor−solid−liquid (VLS) growth mechanism.

ZnS material has been conventionally synthesized by methods like catalytic technique,[12,13] atomic layer deposition,[14] molecular beam epitaxy (MBE),[8] pulsed laser vaporization (PLV),[15] and vapor-phase condensation.[16] However, in most of the previous reports, rather than the band-edge emission in the UV wavelength range, ZnS species always show broad emissions in the wavelength range of 400−550 nm at room temperature which is related to surface states or deep-level defects.[17−19] Up until now, UV emission from ZnS has been sparsely presented, such as ZnS epilayers fabricated on GaAs by MBE[8] and NWs grown by PLV[15] or MBE.[20] Although those reports are encouraging, there is a lack of systematic studies on optical properties of ZnS NWs to provide a clear understanding on the emission mechanisms and the excitonic properties in low dimensionality.

In this research, high crystalline ZnS NWs were synthesized via a PLV technique and their optical properties have been investigated in detail by power-dependent, temperature-dependent photoluminescence (PL) spectroscopy and time-resolved photoluminescence (TRPL) experiments. Exciton emissions and shallow defect-related emission have been observed at low temperatures. Our measurements elucidate the fundamental properties of excitons, such as exciton−phonon interaction and exciton lifetime. A shallow level luminescence is also identified for the first time in ZnS nanowires, which shows a very sensitive dependence to laser excitation power.

The ZnS NWs used herein were grown by the PLV method. Detailed growth conditions are available else-

* To whom correspondence should be addressed, qihua@ntu.edu.sg and hdsun@ntu.edu.sg.

Received for review: 08/24/2010
Published on Web: 11/11/2010

© 2010 American Chemical Society

DOI: 10.1021/nl102987z | *Nano Lett.* **2010,** *10,* 4956–4961

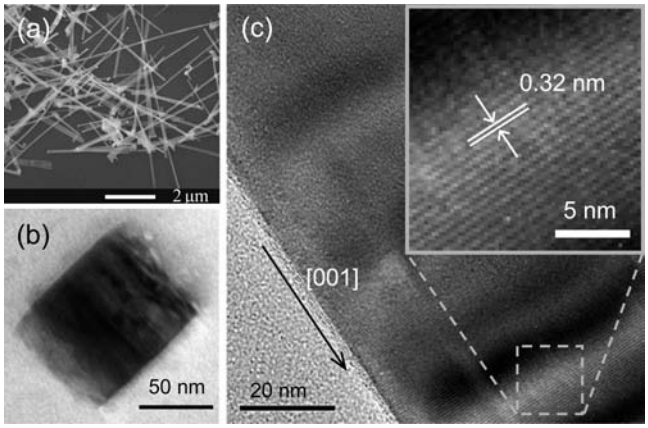

FIGURE 1. SEM and TEM images of ZnS NWs: (a) SEM of ZnS nanowires dispersed on silicon substrate; (b) cross section TEM image of a typical nanowire, revealing nearly spare cross section; (c) HRTEM image of an individual ZnS nanowire grown along the [001] direction.

where.[15] Further characterizations were performed on a JEOL JSM-7001F field emission scanning electron microscope (FESEM) and a JEOL 2010 transmission electron microscope (TEM). The PL measurements were performed between 10 and 300 K within a helium closed-cycle cryostat. A pulsed Nd:YAG fourth harmonic (266 nm) laser was used as the PL excitation source, and the signal was dispersed by a 750 mm monochromator combined with suitable filters and detected by an UV-enhanced charged coupled device (CCD). The pulse width and repetition rate of the laser are about 1 ns and 60 Hz, respectively. TRPL was carried out at room temperature by time-correlated single photon counting (TCSPC) with a resolution of 10 ps (PicoQuant PicoHarp 300), and the 266 nm pulse laser (100 fs, 80 MHz) from the third harmonic of the titanium sapphire laser (Chameleon, Coherent Inc.) was used as an excitation source.

The as-grown NWs were dispersed in ethanol by ultrasonication and then deposited on substrate for further measurements. From the X-ray powder diffraction analysis (not shown here), the sample can be identified to be hexagonal wurtzite phase ZnS NWs. Figure 1a shows the FESEM image of ZnS NWs dispersed on Si substrate. The length of NW was tens of micrometers. With a closer look at the end of some of the NWs, solidified metal particles can be clearly observed, indicating the VLS growth mechanism. As presented in Figure 1b, it is interesting to note that the ZnS NW shows a rectangular or nearly square cross section. On the other hand, the TEM image of the NW in Figure 1c shows that the distance between the adjacent lattice fringes is ~0.32 nm, which indicates highly directional growth of ZnS along the [001] orientation, i.e., *c* axis along wurtzite crystal lattice.

Figure 2 shows the low temperature (10 K) PL spectrum of ZnS NWs under an average excitation density ~9.40 mW/cm^2. Strong UV emission dominates the low temperature spectrum implying the high quality of the sample, while much weaker defect luminescence around 2.50−3.00 eV is not our focus and

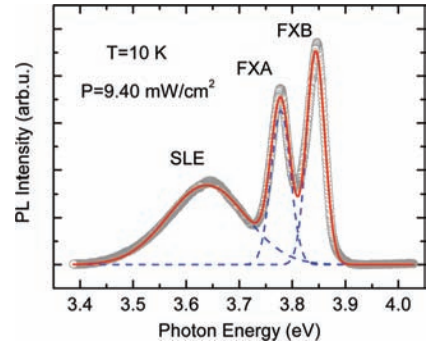

FIGURE 2. The band edge emission spectra of ZnS NWs sample obtained at 10 K. Open circles are the experimental data, and blue dashed lines and a red solid line are the multi-Gaussian fitting of the spectra.

therefore is not presented in this plot. The experimental data (open circles) can be well fitted with the least-squares fit of multiple Gaussians line shape function (solid red curve), which gives rise to accurate values concerning the peak position and full width at half-maximum (fwhm). The blue dashed curves depict the deconvoluted Gaussian bands. In wurtzite ZnS, due to the spin−orbit interaction and crystal field splitting, the topmost valence band splits into three bands and the respective exciton states are denoted as free-exciton A (FXA), B (FXB), and C (FXC). The splitting energies are 89 meV (FXC-FXB) and 57 meV (FXB-FXA), respectively.[7] Thus the observed emissions at 3.778 and 3.844 eV (with an energy difference of 66 meV) can be assigned to FXA and FXB. The absence of FXC may be due to the faster decay. Similar band-edge luminescence doublets have been observed at room temperature,[15] and detailed analysis of the excitonic properties will be presented in the following discussion. On the low energy side, an emission band peaked at 3.639 eV which has never been reported is observed to the best of our knowledge, and we attribute this peak to the shallow level emission (SLE), as will be elaborated later.

Due to the different density of state, the relative intensity of the defect and free exciton transition shows a very different trend by varying excitation densities. Figure 3 depicts the PL spectra measured at 10 K under various excitation densities displayed next to the curves. All the spectra are normalized by the peak intensity of FXB and shifted in *y*-coordinate for better comparison. It is interesting to note that for excitation density increasing by around 2 orders of magnitude, the emission band of SLE demonstrates a faster saturation compared with FXA and FXB and could not be resolved at excitation density higher than 41.0 mW/cm^2. The peak energies of FXA and FXB show a gradual red shift with increased excitation density, while the peak position of SLE is insensitive to photon flux. This may be the reason that this peak was absent in some previous studies,[15] as the excitation power was probably high enough to saturate the SLE. The total shifts from 1.40 to 79.2 mW/cm^2 of FXA and FXB are 8 and 12 meV, respectively. This phenomenon can be ascribed to laser heating effect commonly observed in other nanostructures.[21]

© 2010 American Chemical Society

DOI: 10.1021/nl102987z | *Nano Lett.* **2010,** *10,* 4956–4961

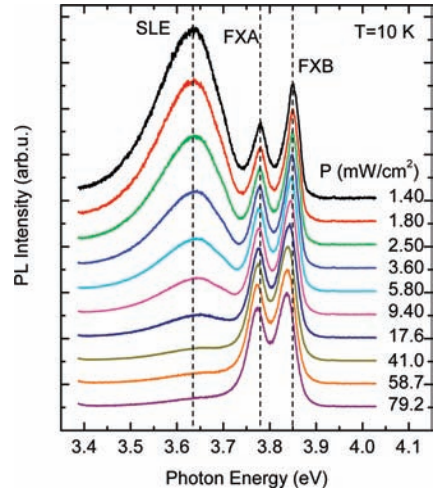

FIGURE 3. Evolution of the PL spectra measured at 10 K under different excitation densities. The dashed vertical lines are a guide for the eyes.

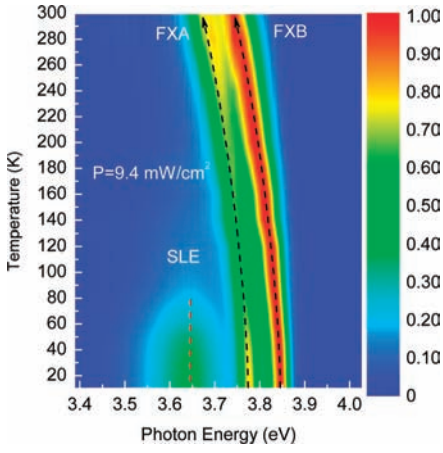

FIGURE 4. Temperature-dependent PL mapping of ZnS NWs sample measured at an excitation density ~9.4 mW/cm². All data were normalized by FXB intensity and the dashed lines follow the peak positions.

At present, the room temperature band gap of ZnS material is still controversial.[8,20,22] The reported data in the previous literature range from 3.560 to as high as 3.764 eV.[8] It is worth mentioning that the laser excitation intensity will influence the determination of the real band gap emission as indicated in Figure 3. Therefore, in order to further investigate the fundamental excitonic properties of ZnS NWs, temperature-dependent PL measurement was carried out under low excitation density ~9.40 mW/cm² to minimize the laser heating effect. The normalized PL spectra of the sample measured at various temperatures are shown in Figure 4. Different peak positions of the individual spectra are indicated by dashed lines. It can be seen that the peak position of SLE remains unchanged, while the PL intensity fades out gradually with increasing temperature, and completely disappears at temperatures higher than 140 K. This verifies our assignment that this peak is related to SLE rather than shallow donor-bound exciton, because otherwise the peak position will show a gradual red shift with increasing temperature.[23] It is also worth noting what shallow donor or acceptor impurities can introduce such SLE levels. Considering the ionization is ~200 mV, one possible contamination NaCl gives rise to shallow Na acceptor or Cl donor level with ionization energies in the range of 170−250 mV.[7] While other intrinsic defects such as Zn vacancy and S interstitial, etc., may not be ruled out, detailed investigation of the origin of the SLE lies beyond the scope of this Letter.

As shown in Figure 4, the emission peaks of FXA and FXB show conventional band gap shrinkage. Compared to Figure 3, the temperature of the sample is around 90 K under excitation density of ~79.2 mW/cm² due to the laser heating effect. The thermal shift of the band gap of the semiconductors is believed to arise from the thermal dilation of the crystal lattice as well as electron−phonon interactions. The temperature dependence of this characteristic can be described by the Varshni formula,[24] or the following Bose−Einstein expression[25]

$$E(T) = E(0) - \frac{\lambda}{\exp(\hbar\bar{\omega}/k_B T) - 1} \quad (1)$$

where $E(0)$ is the band gap at a temperature of 0 K, λ is the proportional coefficient, and $\hbar\bar{\omega}$ is the effective phonon energy. Figure 5a shows the variation of the PL peak energies of FXA and FXB as a function of temperature. Dashed lines are the least-squares fitting curves of the expression to the measured peak values of the FXB spectra at different temperatures and then shift by 66 meV vertically. The fitting parameters obtained are summarized in Table 1, and data for a GaN,[26] ZnO film[27] as well as a ZnSe bulk crystal[28] are also listed for comparison. The peak positions of FXA (FXB) at room temperature and 10 K are 3.676 eV (3.745 eV) and 3.778 eV (3.844 eV). Taking the exciton binding energy of 40 meV into account, the fundamental band gaps deduced from our measurement are 3.716 eV (3.785 eV) and 3.818 eV (3.884 eV) at room temperature and 10 K, respectively, which is in a good agreement with previous reports.[8,15,20]

Thermal broadening of the excitonic peak is generally interpreted as an exciton−phonon interaction. The temperature dependence of fwhm can be approximately described by the following equation[26,29−31]

$$\Gamma(T) = \Gamma_{inh} + \gamma_{ph} T + \frac{\Gamma_{LO}}{[\exp(\hbar\omega_{LO}/k_B T) - 1]} \quad (2)$$

where Γ_{inh}, γ_{ph}, Γ_{LO}, and $\hbar\omega_{LO}$ are the inhomogeneous peak width at zero temperature, the coupling strength of an exciton−acoustic phonon, the coupling strength of an exciton longitudinal optical (LO) phonon, and the LO-phonon energy, respectively. Parts b and c of Figure 5 show the

© 2010 American Chemical Society

DOI: 10.1021/nl102987z | Nano Lett. 2010, 10, 4956–4961

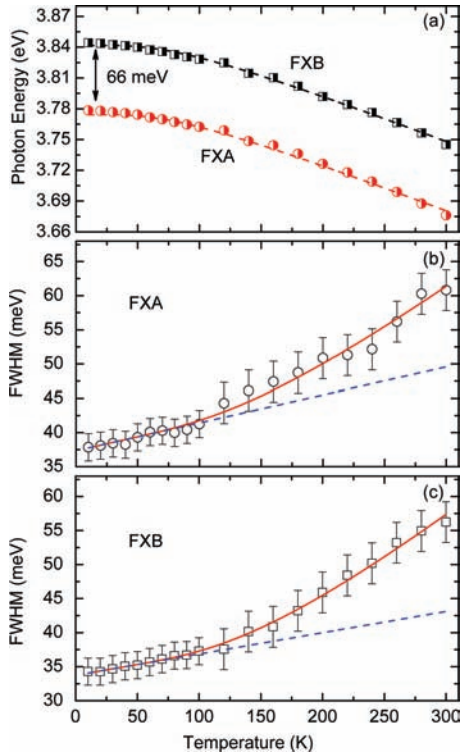

FIGURE 5. (a) Temperature-dependent peak energies and dashed lines are the fitting according to the Bose−Einstein expression. Temperature dependence of the peak widths of FXA (b) and FXB (c), respectively. The solid lines are the fitting of the experimental data based on eq 2, while dashed lines are the contributions from the inhomogeneous broadening and acoustic−phonon scattering.

TABLE 1. E_g is the Band Gap at Room Temperature, E_B is the Exciton Binding Energy, $\hbar\omega_{LO}$ is the LO Phonon Energy, λ is the Proportional Coefficient, $\hbar\bar{\omega}$ is the Effective Phonon Energy, γ_{ph} is the Coupling Strength of Exciton−Acoustic Phonon, and Γ_{LO} the Coupling Strength of Exciton−LO Phonon

material		E_g (eV)	E_B (eV)	$\hbar\omega_{LO}$ (meV)	λ (meV)	$\hbar\bar{\omega}$ (meV)	γ_{ph} (μeV/K)	Γ_{LO} (meV)
ZnS	FXA	3.716	40	42.95	108.40	19.89	40.78	50.40
	FXB	3.785					31.23	60.85
GaN[a]	FXA	3.42	26	91.5	121.00	27.30	21	525
	FXB						22	495
ZnO[b]	FXA	3.37	60	72	20.90	11.44	11.3	876.1
	FXB				11.48	21.80	26.5	783.3
ZnSe[c]		2.69	19	31.4	32.10	9.90	64.2	126

Note: [a] Reference 26. [b] Reference 27. [c] Reference 28.

temperature dependence of the fwhm of the FXA and FXB, respectively. Solid lines represent the fitting results based on eq 2. It is found that a reasonably good fit is obtained, and the results are summarized in Table 1. Here, we have taken the LO phonon energy $\hbar\omega_{LO} = 42.95$ meV for each fitting, which is obtained from previous Raman measurements (346.4 cm^{-1}).[32,33] In parts b and c of Figure 5, the dashed lines are the contributions from the inhomogeneous broadening and acoustic−phonon scattering ($\Gamma(T) = \Gamma_{inh} + \gamma_{ph}T$). It is noted that the acoustic−phonon contributes up to 120 K very significantly, but the contribution from LO phonon is negligible up to this temperature. From 120 K

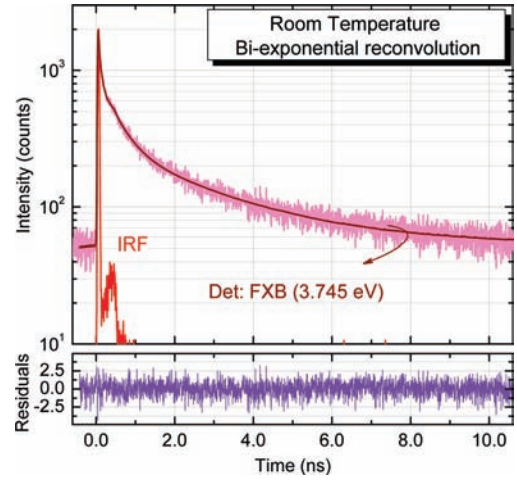

FIGURE 6. Room temperature TRPL data for ZnS NWs monitored at FXB. Solid curves are the fitting according to eq 3, and the separate plot shows the weighted residuals during the reconvolution.

onward the participation of the LO phonon causes the fwhm to increase further.

The exciton−LO phonon coupling strength (Γ_{LO}) for FXA and FXB deduced from the fitting is comparable. However, those parameters are quite small compared to the other wide band gap materials like GaN, ZnO, and ZnSe. As is well-known, the exciton line width broadening is due to a 1S exciton either dissociating into the free-electron−hole continuum or scattering within the discrete exciton band by absorbing one LO phonon via the Fröhlich interaction. Here, Γ_{LO} is related to materials polarity and the magnitude of the exciton binding energy relative to the LO-phonon energy.[29] It can be seen from Table 1 that the exciton binding energy and the LO-phonon energy of ZnS are comparable. Therefore, the dissociation of the 1S exciton into continuum states is suppressed and Γ_{LO} is small. We would like to emphasize that the small value of Γ_{LO} implies that excitons are less probable to be disassociated by LO phonons. So excitons in ZnS are very stable even though the exciton binding energy in ZnS is not as high as that of ZnO, which is a good merit for excitonic light-emitting devices.

In order to determine the free-carrier or exciton lifetime, an important parameter related to material quality and device performance, TRPL was carried out at room temperature. Figure 6 shows the TRPL data for ZnS NWs monitored at the peak of FXB. The decay curve can be well fitted by a biexponential fit with reconvolution

$$I(t) = \int_{-\infty}^{t} \mathrm{IRF}(t') \sum_{i=1}^{2} A_i e^{-(t-t')/\tau_i}\, dt' \qquad (3)$$

where A_i is the amplitude of the ith component at time zero, τ_i is the corresponding lifetime, and IRF is the instrument response function. A separate plot shows the weighted

© 2010 American Chemical Society

DOI: 10.1021/nl102987z | Nano Lett. 2010, 10, 4956–4961

TABLE 2. Decay Constants and the Amplitudes Obtained from the Fitting Based on Equation 3

					fractional intensity (%)	
detection energy (eV)	A_1	τ_1 (ns)	A_2	τ_2 (ns)	τ_1	τ_2
3.815	0.71	0.42	0.29	2.66	27.9	72.1
3.745 (FXB)	0.71	0.43	0.29	2.61	28.7	71.3
3.676 (FXA)	0.72	0.48	0.28	2.71	31.3	68.7
3.615	0.72	0.46	0.28	2.68	30.6	69.4

residuals, and the straight line indicates a good fit. Table 2 summarizes the decay constants and the amplitudes obtained from the fits for varying detection wavelengths. It can be seen that all the detected wavelengths exhibit similar carrier dynamics. The fast decay component τ_1 is ~0.45 ns, and the slow decay component τ_2 is ~2.7 ns. The biexponential behavior strongly suggests that two different species are involved in the emission.

The biexponential decay of the PL could be explained by exciton diffusion from the surface region to the bulk region. It is expected that excitons diffuse away from the surface while simultaneously undergoing nonradiative recombination and emitting exciton luminescence. These processes were presumed to occur on a fast time scale and would correspond to the fast component of the PL decay, whereas the slow component would correspond to relaxation once the excitons have diffused and equilibrated throughout the volume of the ZnS NW.[34] However, due to the large absorption coefficient of ZnS at the excitation energy ($\alpha_{exc} = 2.5 \times 10^5$ cm^{-1}),[35,36] the effective penetration depth of optical excitation is estimated to be ~40 nm. Note that the penetration depth is comparable to the diameter of the ZnS NWs as depicted in Figure 1b, and thus the carriers are expected to generate uniformly throughout the whole NW. Therefore, the surface-bulk diffusion can be excluded for the reason of biexponential decay.

Compared to the reported data, the fast decay component is comparable to what has been measured for bulk ZnO ($\tau_{fast}^{bulk} \sim 0.43$ ns) and has been associated with nonradiative recombination.[37] The nonradiative process here is considered to be generated by certain defect species such as nonradiative surface traps. The fast decay component is much more prominent for ZnS NWs ($A_1 \sim 0.7$) compared to bulk single-crystal ZnO ($A \sim 0.3$).[34,37] Generally speaking, in the case of NW, as the sample's surface-to-volume ratio increases, the relative density of nonradiative surface traps would increase and the weight of the fast decay component (associated with free exciton plus nonradiative surface recombination) would increase. For the slow decay component for ZnS NWs, the decay time ~2.7 ns can be attributed to the intrinsic radiative lifetime of the free exciton. This value is comparable to bulk single-crystal ZnO which is ~3 ns.[37] From the decay constants and the amplitudes listed in Table 2, the relative fractional intensity ($A_i\tau_i$) of each component can be determined. It can be seen that the slow decay component is the dominant contribution to the whole PL intensity, which confirms our assignment that it is related to the effective free exciton lifetime.

In conclusion, we have synthesized high crystalline quality ZnS NWs by the PLV method. Systematic optical measurements allow us to identify the emission origins from FXA, FXB, and SLE. The exciton−phonon interaction in ZnS NWs is relatively weak, evidenced by slow temperature dependence of broadening of the PL emission bands. The physical implication is that the small LO phonon energy relative to the exciton binding energy leads to small probability of exciton disassociation by LO phonons. Therefore, excitons in ZnS can robustly exist even at room temperature, which ensures high efficiency excitonic emission. Considering their lower density of crystalline defects, ZnS nanowires can be envisaged as a potential material for technically important UV light emitter at nanoscale. Finally, the carrier dynamics of the ZnS NWs at room temperature was analyzed and the radiative lifetime of the free exciton was estimated. Our results provide detailed excitonic properties of ZnS NWs and point out that it can serve as an excellent UV functional material. Research down this line may help to advance UV photonic and sensing devices based on ZnS NWs.

REFERENCES AND NOTES

(1) Huang, M. H.; Mao, S.; Feick, H.; Yan, H. Q.; Wu, Y. Y.; Kind, H.; Weber, E.; Russo, R.; Yang, P. D. *Science* **2001**, *292* (5523), 1897–1899.

(2) Wang, X. D.; Summers, C. J.; Wang, Z. L. *Nano Lett.* **2004**, *4* (3), 423–426.

(3) Tang, Z. K.; Wong, G. K. L.; Yu, P.; Kawasaki, M.; Ohtomo, A.; Koinuma, H.; Segawa, Y. *Appl. Phys. Lett.* **1998**, *72* (25), 3270–3272.

(4) Soci, C.; Zhang, A.; Xiang, B.; Dayeh, S. A.; Aplin, D. P. R.; Park, J.; Bao, X. Y.; Lo, Y. H.; Wang, D. *Nano Lett.* **2007**, *7* (4), 1003–1009.

(5) Zhao, Y. W.; Zhang, Y.; Zhu, H.; Hadjipianayis, G. C.; Xiao, J. Q. *J. Am. Chem. Soc.* **2004**, *126* (22), 6874–6875.

(6) Zhao, J.; Wang, A.; Altermatt, P.; Green, M. A. *Appl. Phys. Lett.* **1995**, *66* (26), 3636–3638.

(7) Blachnik, R.; Chu, J.; Gałazka, R. R.; Geurts, J.; Gutowski, J.; Hoenerlage, B.; Hofmann, D.; Kossut, J.; Levy, R.; Michler, P.; Neukirch, U.; Strauch, D.; Story, T.; Waag, A. *Landolt-Börnstein: Numerical data and functional relationships in science and technology*. New Series Edition; Rössler, U., Ed.; Springer-Verlag: Berlin, Germany, 1999; Vol. III/41B.

(8) Tran, T. K.; Park, W.; Tong, W.; Kyi, M. M.; Wagner, B. K.; Summers, C. J. *J. Appl. Phys.* **1997**, *81* (6), 2803–2809.

(9) Ma, C.; Moore, D.; Li, J.; Wang, Z. L. *Adv. Mater.* **2003**, *15* (3), 228–231.

(10) Peng, H.; Makarona, E.; He, Y.; Song, Y. K.; Nurmikko, A. V.; Su, J.; Ren, Z.; Gherasimova, M.; Jeon, S. R.; Cui, G.; Han, J. *Appl. Phys. Lett.* **2004**, *85* (8), 1436–1438.

(11) McGuinness, C. D.; Sagoo, K.; McLoskey, D.; Birch, D. J. S. *Appl. Phys. Lett.* **2005**, *86* (26), 261911–261913.

(12) Ding, J. X.; Zapien, J. A.; Chen, W. W.; Lifshitz, Y.; Lee, S. T.; Meng, X. M. *Appl. Phys. Lett.* **2004**, *85* (12), 2361–2363.

(13) Jiang, Y.; Meng, X. M.; Liu, J.; Hong, Z. R.; Lee, C. S.; Lee, S. T. *Adv. Mater.* **2003**, *15* (14), 1195–1198.

(14) Farhangfar, S.; Yang, R. B.; Pelletier, M.; Nielsch, K. *Nanotechnology* **2009**, *20* (32), 325602.

(15) Xiong, Q.; Chen, G.; Acord, J. D.; Liu, X.; Zengel, J. J.; Gutierrez, H. R.; Redwing, J. M.; Lew Yan Voon, L. C.; Lassen, B.; Eklund, P. C. *Nano Lett.* **2004**, *4* (9), 1663–1668.

© 2010 American Chemical Society

DOI: 10.1021/nl102987z | *Nano Lett.* **2010,** *10,* 4956–4961

(16) Yuan, H. J.; Xie, S. S.; Liu, D. F.; Yan, X. Q.; Zhou, Z. P.; Ci, L. J.; Wang, J. X.; Gao, Y.; Song, L.; Liu, L. F.; Zhou, W. Y.; Wang, G. *J. Cryst. Growth* **2003**, *258* (3−4), 225–231.
(17) Denzler, D.; Olschewski, M.; Sattler, K. *J. Appl. Phys.* **1998**, *84* (5), 2841–2845.
(18) Wang, Y.; Zhang, L.; Liang, C.; Wang, G.; Peng, X. *Chem. Phys. Lett.* **2002**, *357* (3−4), 314–318.
(19) Zhu, Y. C.; Bando, Y.; Xue, D. F. *Appl. Phys. Lett.* **2003**, *82* (11), 1769–1771.
(20) Chan, S. K.; Lok, S. K.; Wang, G.; Cai, Y.; Wang, N.; Sou, I. K. *J. Electron. Mater.* **2008**, *37* (9), 1344–1348.
(21) Yang, Y.; Yan, H.; Fu, Z.; Yang, B.; Xia, L.; Xu, Y.; Zuo, J.; Li, F. *J. Phys. Chem. B* **2005**, *110* (2), 846–852.
(22) Lippens, P. E.; Lannoo, M. *Phys. Rev. B* **1989**, *39* (15), 10935–10942.
(23) Chen, R.; Xing, G. Z.; Gao, J.; Zhang, Z.; Wu, T.; Sun, H. D. *Appl. Phys. Lett.* **2009**, *95* (6), No. 061908−3.
(24) Varshni, Y. P. *Physica (Amsterdam)* **1967**, *34* (1), 149–154.
(25) Lautenschlager, P.; Garriga, M.; Logothetidis, S.; Cardona, M. *Phys. Rev. B* **1987**, *35* (17), 9174–9189.
(26) Viswanath, A. K.; Lee, J. I.; Kim, D.; Lee, C. R.; Leem, J. Y. *Phys. Rev. B* **1998**, *58* (24), 16333–16339.
(27) Makino, T.; Chia, C. H.; Tuan, N. T.; Segawa, Y.; Kawasaki, M.; Ohtomo, A.; Tamura, K.; Koinuma, H. *Appl. Phys. Lett.* **2000**, *76* (24), 3549–3551.
(28) Bogani, F.; Carraresi, L.; Filoramo, A.; Savasta, S. *Phys. Rev. B* **1992**, *46* (15), 9461–9468.
(29) Sun, H. D.; Makino, T.; Tuan, N. T.; Segawa, Y.; Kawasaki, M.; Ohtomo, A.; Tamura, K.; Koinuma, H. *Appl. Phys. Lett.* **2001**, *78* (17), 2464–2466.
(30) O' Neill, M.; Oestreich, M.; Rühle, W W.; Ashenford, D. E. *Phys. Rev. B* **1993**, *48* (12), 8980–8985.
(31) Sun, H. D.; Makino, T.; Segawa, Y.; Kawasaki, M.; Ohtomo, A.; Tamura, K.; Koinuma, H. *J. Appl. Phys.* **2002**, *91* (4), 1993–1997.
(32) Xiong, Q. H.; Wang, J. G.; Reese, O.; Voon, L.; Eklund, P. C. *Nano Lett.* **2004**, *4* (10), 1991–1996.
(33) Adu, K. W.; Xiong, Q.; Gutierrez, H. R.; Chen, G.; Eklund, P. C. *Appl. Phys. A: Mater. Sci. Process.* **2006**, *85* (3), 287–297.
(34) Foreman, J. V.; Everitt, H. O.; Yang, J.; Liu, J. Carrier dynamics and photoexcited emission efficiency of ZnO:Zn phosphor powders In *Ultrafast Phenomena in Semiconductors and Nanostructure Materials XIII*; Proceedings of SPIE; Tsen, K.-T., Song, J.-J., Betz, M., Elezzabi, A. Y., Eds.; SPIE: San Jose, CA, USA, 2009; Volume 7214, Paper Number 721405.
(35) Ong, H. C.; Chang, R. P. H. *Appl. Phys. Lett.* **2001**, *79* (22), 3612–3614.
(36) Ozaki, S.; Adachi, S. *Jpn. J. Appl. Phys., Part 1* **1993**, *32* (11A), 5008–5013.
(37) Teke, A.; Özgür, Ü.; Doğan, S.; Gu, X.; Morkoç, H.; Nemeth, B.; Nause, J.; Everitt, H. O. *Phys. Rev. B* **2004**, *70* (19), 195207.

© 2010 American Chemical Society

DOI: 10.1021/nl102987z | *Nano Lett.* **2010,** *10,* 4956–-4961